4. Extreme Ultraviolet Survey

Experiment MA-083

S. Bowyer,[a†] B. Margon,[a] M. Lampton,[a] F. Paresce,[a] and R. Stern[a]

ABSTRACT

A grazing incidence telescope sensitive to radiation in the 5- to 100-nm band was flown in the Apollo service module. On 10 nighttime revolutions, the command and service module was maneuvered to point the instrument at 30 different stellar targets for periods of 1 to 20 minutes, thus constituting the first sensitive search for extreme ultraviolet radiation from nonsolar sources. Several hours of supplementary data were also obtained during nighttime orbits when other experiments in the scientific instrument bay were operating.

Analysis of the data completed thus far indicates the definite detection of at least four extrasolar extreme ultraviolet sources. The probable identifications of these sources are the hot white dwarfs HZ 43 and Feige 24, the dwarf nova SS Cygni, and the M-dwarf flare star Proxima Centauri. The two white dwarfs are the most intense sources, with fluxes incident at Earth of 3 to 4 pW/m^2 in the 17- to 62-nm band. Optical spectrophotometric measurements of these two objects made with the 3-m telescope at the Lick Observatory have been combined with the extreme ultraviolet data to derive several physical parameters of the stars; the investigators found these two objects to be the hottest and the most luminous known white dwarfs. The shapes of their extreme ultraviolet spectra may be used to infer that the density of the local neutral component of interstellar hydrogen is $\lesssim 0.02$ atom/cm^3, which is promising for future astronomical observations in this wavelength band.

The four objects thus far identified are the first extrasolar sources to be detected in the extreme ultraviolet band. Computer analysis of both the prime and supplementary data will eventually yield near-photon-limited sensitivity levels for coverage over a considerable fraction of the July night sky and may reveal additional point sources. These observations also provide the largest volume of data ever obtained on the ultrasoft component of the diffuse cosmic X-ray background. Preliminary analysis of these data indicates that spatial isotropy is restored in the 6- to 15-nm band, contrary to the well-known anisotropy of the 4.4- to 6-nm radiation.

INTRODUCTION

Astronomical observations of nonsolar sources in the extreme ultraviolet (EUV) region of the electromagnetic spectrum (10 to 100 nm) are of profound significance for studies of stellar evolution, stellar atmospheres, and the interstellar medium. The existence of stars producing predominantly ionizing radiation (wavelengths less than 91.2 nm) has been postulated to explain the ionization state of the interstellar medium. Such stars might represent a very hot phase of stellar evolution (refs. 4-1 and 4-2). Effective surface temperatures greater than 20 000 K have been observed, for example, among O stars, among white dwarfs of classes DAn and DAwk, among the

[a]University of California at Berkeley.

[†]Principal Investigator.

subdwarf OB stars (ref. 4-3), and among the ultraviolet (UV) excess objects observed from the European TD-1A satellite (ref. 4-4). A major deterrent to previous attempts at celestial EUV observations has been the opacity of the interstellar gas resulting from photoelectric absorption by neutral hydrogen and neutral and singly ionized helium. However, recent spectroscopic studies of interstellar matter toward nearby stars (refs. 4-5 to 4-7) indicate that, in many directions, neutral hydrogen concentrations are as low as 0.01 to 0.1 atom/cm^3. Then, the absorption cross sections given in reference 4-8 indicate that direct EUV observations of sufficiently hot stars should be possible to distances of 20 to 100 pc.

Preliminary surveys at EUV wavelengths have been made from sounding rockets and have set upper limits of approximately 0.1 nW/m^2 for sources in limited regions of the sky (refs. 4-9 to 4-13). However, significant constraints on stellar emission models would require improvements in sensitivity of perhaps two orders of magnitude. The Apollo-Soyuz mission offered the opportunity to make extended observations of numerous candidate stars with an EUV telescope that had the requisite sensitivity. Ten nighttime orbits were used to obtain data on 30 preselected stars, 1 planet, and the EUV background radiation.

EQUIPMENT

The EUV telescope (ref. 4-14) consisted of a 37-cm-diameter grazing incidence mirror assembly, a continually rotating (10 rpm) six-position filter wheel, and a pair of channel electron multiplier detectors. A schematic view of the instrument is shown in figure 4-1.

The parabolic optics were fabricated from aluminum coated with a nickel alloy and then overcoated with a fine layer of gold. The filter wheel included an opaque filter that permitted nearly continuous monitoring of the detector background during the mission. The field of view (FOV) of the instrument was circular with selectable diameters of 2.5° or 4.3° full width at half maximum obtained by commanding either detector into the focal position. The detailed construction of the detector modules is described in reference 4-15. The detector not at the focal position was also monitored to further establish the stability of the background count rates. Count rates from both detectors were telemetered each 0.1 second together with the filter wheel position and other auxiliary information.

The entire system was calibrated in the laboratory with collimated radiation at numerous wavelengths between 4.4 and 265 nm. Absolute intensities were established by using National Bureau of Standards-calibrated vacuum-photodiode secondary standards above 20 nm and propane proportional counters below 20 nm. The various filters, in combination with the efficiency characteristics of the mirror assembly and detector, defined the wavelength bands illustrated in figure 4-2. The detailed response of the system is summarized in table 4-I. The filters and their band passes at 10 percent of peak transmission, the energy-integrated effective area, or grasp $G = \int A(E)\,dE$ (where E is energy and A is area), and the effective energy $E_e = \int EA(E)\,dE/G$ are given in table 4-I.

The experiment was mounted to a shelf in bay 1 of the service module (SM). A protective cover enclosed the instrument assembly at all times when the experiment was not in operation. At appropriate times in the Flight Plan, the crew activated a switch in the command module (CM) to open the cover. The remaining experiment controls consisted of a POWER ON/OFF switch and a two-position detector-selection switch. Both switches were located in the CM and operated by the crew.

The observing procedure consisted of opening the experiment cover, waiting 10 seconds to permit the ambient pressure in the SM bay to vent to vacuum, and then turning the instrument power on. The crewmember then selected the appropriate detector to ensure that the proper channel multiplier was always in the focal plane. The filter wheel operated automatically and continuously whenever the instrument power was on.

The telescope was oriented at preselected targets by using the spacecraft command module computer (CMC) for guidance and orientation and by using the normal Apollo reaction control system thrusters for maneuverability to point the

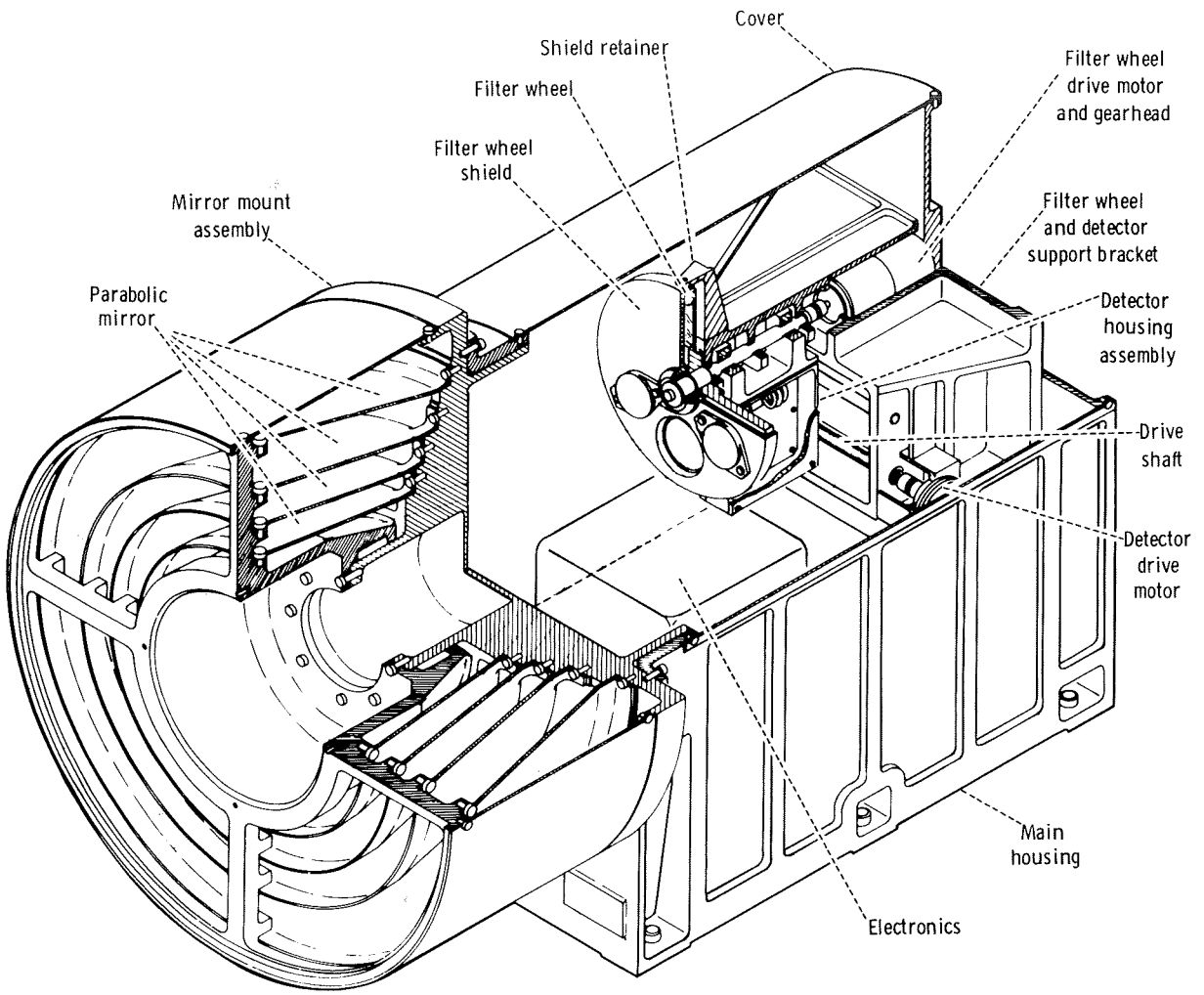

FIGURE 4-1.—A schematic diagram of the EUV telescope.

instrument line of sight at the desired position on the celestial sphere for predetermined lengths of time. The typical target observation sequence consisted of spending equal amounts of time pointing at a target and at two background points located 3° on each side of the target. Any statistically significant differences between the average count rates when observing target and background are then attributable to EUV emission from the object under study. Target observations lasting from 1 to 20 minutes were executed.

RESULTS

The EUV telescope functioned perfectly during the entire mission. The background count rates remained low and reproducible, and the data show no evidence of degradation in instrument sensitivity from the laboratory-measured values.

On revolution 65 at 108 hours 26 minutes ground elapsed time, a preplanned raster scan maneuver was executed using a special erasable memory program in the CMC. This maneuver

consisted of slewing the telescope in a zigzag pattern back and forth across a star of known brightness in the far UV (≈130 nm) where the barium fluoride filter has maximum sensitivity. Because the target position is known in celestial coordinates, a comparison of the time history of the barium fluoride count rates during this maneuver with the known command and service module (CSM) attitude enables the calculation of the actual (in-flight) alinement of the experiment with respect to the CM inertial measuring unit. This information could then be used to recompute CSM pointing data for mission targets to compensate for any changes in alinement from the nominal values caused by vibration or thermal stresses. However, analysis of the revolution 65 raster scan data, obtained on the stars ι Aql and κ Aql, indicated, to an accuracy of 0.3°, that no change from the nominal alinement occurred.

Observation of the targets proceeded normally with occasional small deviations from the observing list caused by time-line anomalies. The rationale for target selection is discussed in reference 4-14. A list of the targets actually observed appears in table 4-II. This list is composed of 30 distinct targets. Seven targets were observed twice during the mission, one target was observed three times, and one target was observed during an extended crew sleep period while the spacecraft was in a fixed inertial attitude.

During the mission, considerable real-time planning enabled additional high-quality science data to be obtained. For example, on day 4 of the mission, the American Association of Variable Star Observers advised that the dwarf nova SS Cygni had undergone an optical outburst. As a result, additional observations of this target were obtained on revolutions 80 and 105. Similarly, several nighttime revolutions originally intended for observing soft X-ray targets became available for the EUV survey because of difficulties with the soft X-ray experiment.

The results of the observations on targets of particular interest are given in the following discussion.

HZ 43

As part of the preplanned observing schedule, on revolution 109 the ultrasoft X-ray source in Coma Berenices (refs. 4-16 to 4-18) was observed for 7 minutes starting at 22:26 UT on July 22, 1975. After taking background data for 1 minute, a 3° spacecraft roll maneuver brought the center of the instrument line of sight to a point 1° north of the intended target. Thus, the target was just at the edge of the 2° FOV of the instrument. Several roll and pitch motions of approximately 0.5° resulted from spacecraft motion within the attitude deadband box and moved the FOV off and on the source. Finally, additional sky background data were obtained 3° off the target.

During these maneuvers, obvious increases and decreases in the detector count rates were immediately recognized. A plot of the count rate as opposed to time is shown in figure 4-3 for the 5.5 to 15, 11.4 to 15, 17 to 62, 50 to 78, and 135 to 154 nm bands with each point representing the

TABLE 4-I.—EUV Instrument Characteristics

Filter material	*Band pass*		*Grasp, cm^2 eV*	*Effective energy, eV*
	eV	*nm*		
Parylene N	83 to 225	5.5 to 15.0	590	142
Beryllium/ parylene N	83 to 109	11.4 to 15.0	60	100
Aluminum plus carbon	20 to 73	17 to 62	270	46
Tin	16 to 25	50 to 78	108	21
Barium fluoride	8.0 to 9.2	135 to 154	.47	9

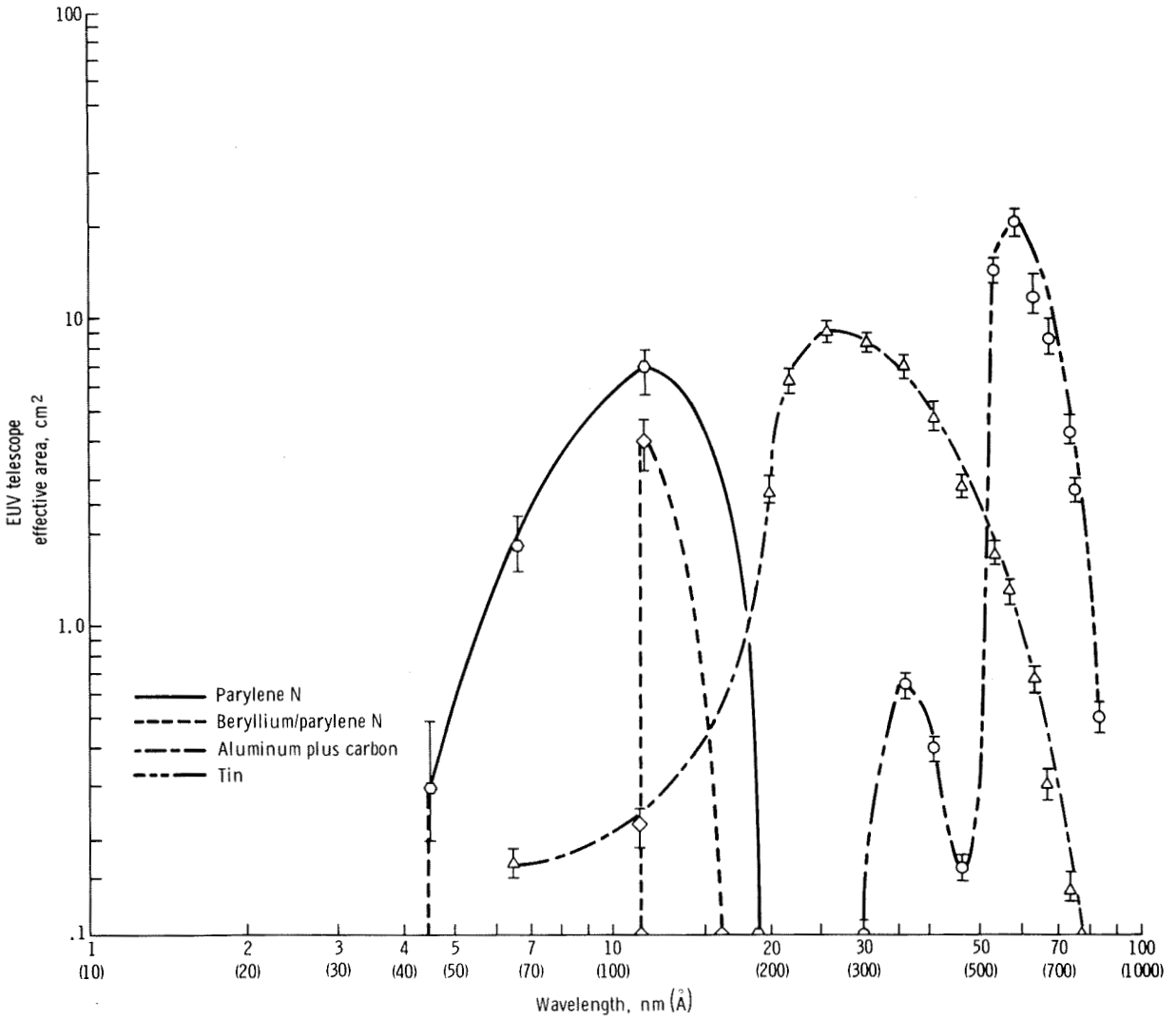

FIGURE 4-2.—Effective area of the EUV telescope as determined by the laboratory calibration data. (The response of the barium fluoride band pass, which was used primarily for instrument alinement determination, is given in table 4-I.)

average count rate during an 0.8-second time interval. Also shown is the count rate in the opaque filter position, which indicates that the observed instrumental background remained steady at 0.6 count/sec.

A crude estimate of the spectral energy distribution of an object can be made by dividing the observed count rate in each band by the appropriate energy-integrated effective area. Such an estimate is exact for continua having constant photon fluxes per unit frequency. Listed in table 4-III are the observed background-subtracted count rates for the Coma source, corrected for atmospheric attenuation at E_e based on the Committee on Space Research International Reference Atmosphere 1965 model 2 reference atmosphere, appropriate for the observing conditions. The total energy flux in the 17- to 62-nm band is approximately 4 pW/m^2.

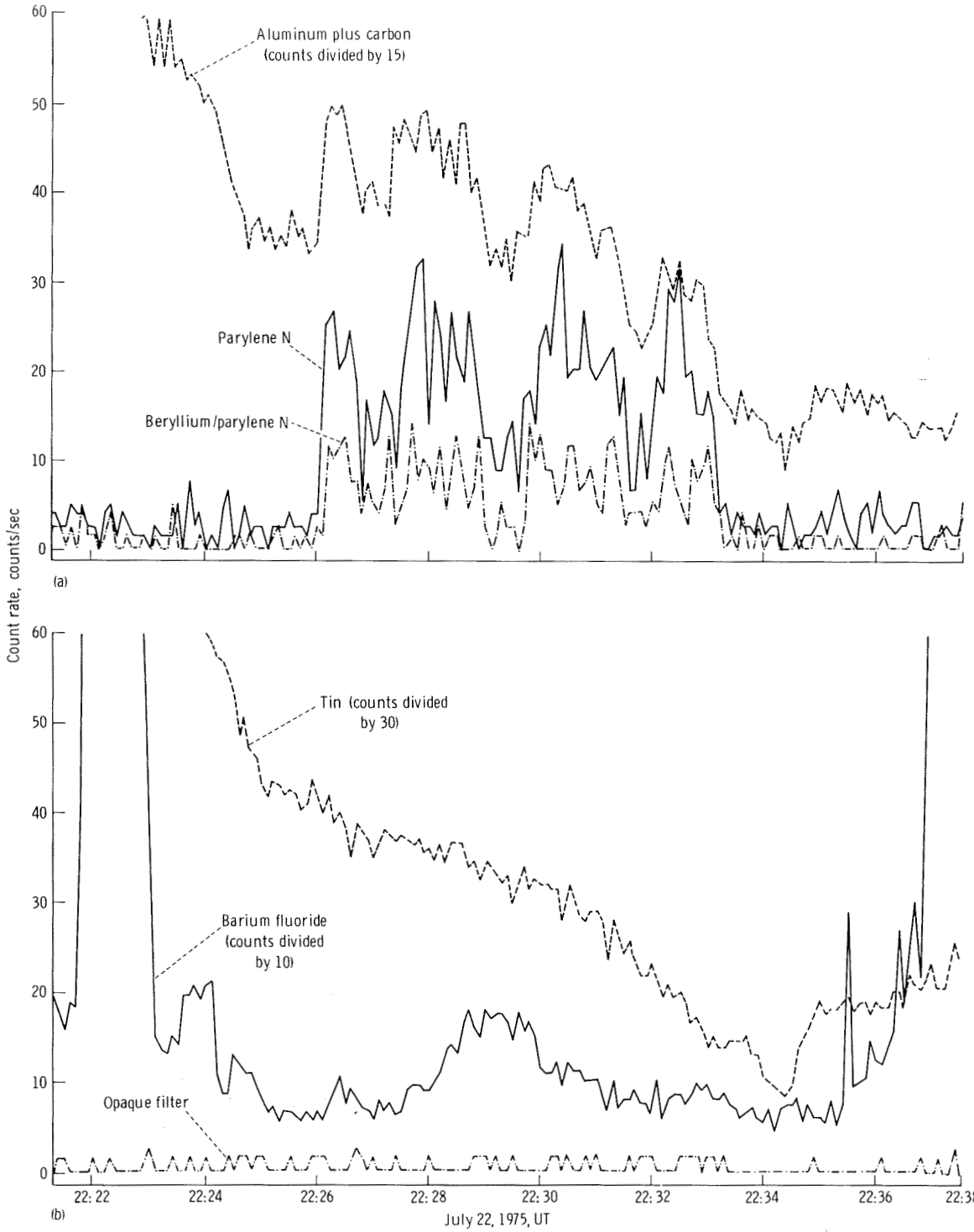

FIGURE 4-3.—The EUV data obtained during a portion of revolution 109. The trends in the aluminum and tin band passes are due to the spatial variations in the geocoronal foreground radiation. This behavior was repeated on numerous orbits. The barium fluoride count rates are dominated by the occasional observations of known blue stars. (a) Aluminum plus carbon, parylene N, and beryllium/parylene N. (b) Tin, barium fluoride, and the opaque filter.

TABLE 4-II.—Targets Observed by the EUV Telescope

Revolution	*Target*
72	EV Lac, AE Aqr, NGC 7293, ϵ Eri
73	VW Cep, DQ Her, 70 Oph, α PsA
80	EV Lac, SS Cyg, DQ Her, θ Oph, α Cen
88	α CMa B
89	NGC 6853, PSR 1929+10, α Aql, UV Cet, Feige 24
90	SS Cyg, 61 Cyg, BD +28°4211, Jupiter
94	HZ 29, i Boo, Prox Cen
105	SS Cyg, BD +28°4211
108	Wolf 424, α Cen, Z Cha, VW Hyi, UV Cet
109	PSR 1133+16, HZ 43, Prox Cen, PSR 1451−68, β Hyi
113 to 117	Wolf 424

TABLE 4-III.—EUV Photometry of Selected Targets

Object	*Revolution*	*Length of exposure, sec*	*Count rate,* [a] *counts/sec*				
			Parylene N	*Beryllium/ parylene N*	*Aluminum plus carbon*	*Tin*	*Barium fluoride*
Positive detections							
HZ 43	109	427	23 ± 1	9 ± 0.6	270 ± 5	<130	<25
	104	9	25 ± 5	7 ± 3	240 ± 25	--	<80
Feige 24	89	125	2 ± 1	<1	232 ± 5	<65	<150
Proxima Centauri	109	78	4 ± 1	<1.5	<45	<120	--
	94	1100	1 ± 1	<1	<50	--	--
SS Cygni	80	135	2 ± 0.5	<1	<45	<125	<150
	90	103	1 ± 0.5	<1	<52	<120	<180
	105	372	<1	<1	<45	<80	<150
Upper limits							
Sirius B	88	74	<2.5	<2.0	<350	<625	<54 400
Jupiter	90	322	<2	<1	<70	<160	<90
PSR 1133+16	109	75	<4	<2.5	<160	<150	<960
PSR 1451−68	109	329	<5	<4	<60	<120	<240
PSR 1929+10	89	252	<2	<2	<40	<90	<120
Hercules X−1	104	582	<1	<1	<45	<180	<60

[a] All count rates are corrected for background and atmospheric absorption. No entry indicates rapidly changing background, short exposure, or South Atlantic Anomaly precluded useful upper limit. Rates may be converted to photon fluxes by using data in table 4-I.

The intensities of this source have been plotted as a function of wavelength in figure 4-4. Also shown is the 4.4- to 16.5-nm detection and 1-keV upper limit in reference 4-17. The data appear compatible and support the identification of the EUV object with the Coma soft X-ray source. Figure 4-4 clearly indicates that the spectrum peaks in the EUV band at approximately 30 nm.

Positional information on this source can be derived from the fact that, as the spacecraft pointing varies, the count rates are occasionally interrupted. Telemetered data on the CSM aspect have been combined with in-flight data on the experiment alinement to obtain four independent position zones for the source. These zones define a common region that is shown in figure 4-5 superposed on the relevant star field.

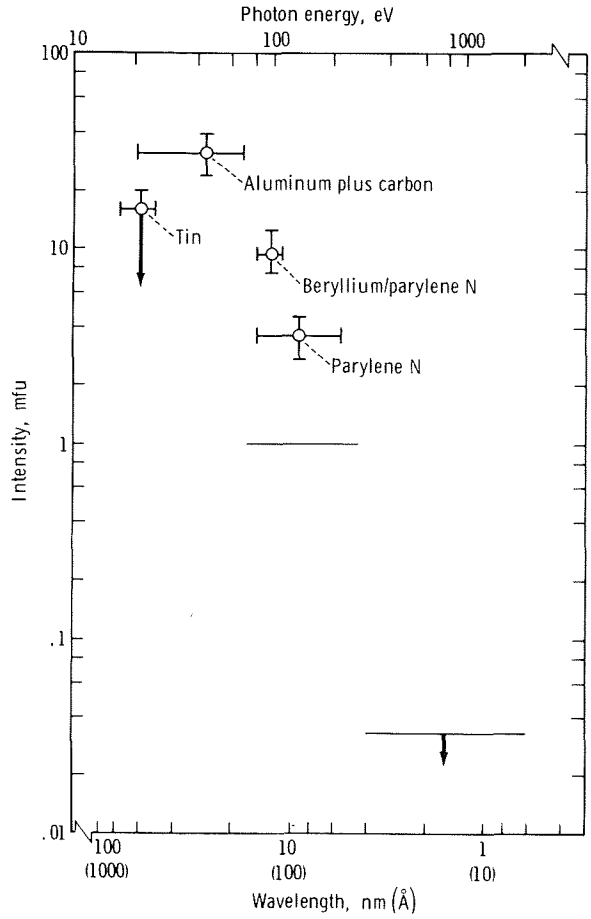

FIGURE 4-4.—Spectral intensities derived from the EUV data on the source in Coma Berenices. Soft X-ray data (ref. 4-17) are also shown.

The Small Astronomy Satellite-3 observations reported in reference 4-18 have given a positional error box for the soft X-ray source that is compatible with the EUV position and is also shown in figure 4-5. It is highly probable that one object is responsible for the soft X-ray and EUV emissions. It has been suggested (ref. 4-18) that the soft X-ray object is the hot white dwarf HZ 43 at α (1950) = $13^h14.0^m$, δ (1950) = +29°22′. This object is also marked on figure 4-5, and the EUV position is compatible with this suggestion.

Without assumption as to the optical identification of the source, a description of the spectrum may be provided by using the observed count rates to constrain parameters of emission models. The simple continuum models chosen for these calculations had photon number per unit energy functions of the following forms: power law, $N(E) = cE^n \exp(-N_H\sigma)$; exponential, $N(E) = cE^{-1}\exp(-E/kT)\exp(-N_H\sigma)$; and black body, $N(E) = cE^2[\exp(E/kT) - 1]^{-1}\exp(-N_H\sigma)$; where N is photon number, c is intensity coefficient, T is temperature, k is the Boltzmann constant, n is the photon power-law index, and N_H is the column density of neutral interstellar hydrogen. In each case, the energy-dependent absorption cross section per hydrogen atom σ has been taken from reference 4-8 with normal abundances, no ionization, and no molecular hydrogen.

The collected data can be satisfactorily fit by any of these trial spectra provided that the free parameters are appropriately chosen. Figure 4-6 shows the derived parameter constraints for these models. In each case, contours are drawn at the χ^2_{min} + 6.25 level appropriate for 90 percent statistical confidence with three free parameters (ref. 4-19). These constraints are compatible with, but much stricter than, the parameter regions derived from the soft X-ray rocket data given in reference 4-17.

Because of the strong likelihood of the association of this EUV source with the stellar system HZ 43, the investigators have obtained correlative ground-based data on the optical object using the facilities of the Lick and Allegheny Observatories. The HZ 43 system is known to consist of a very

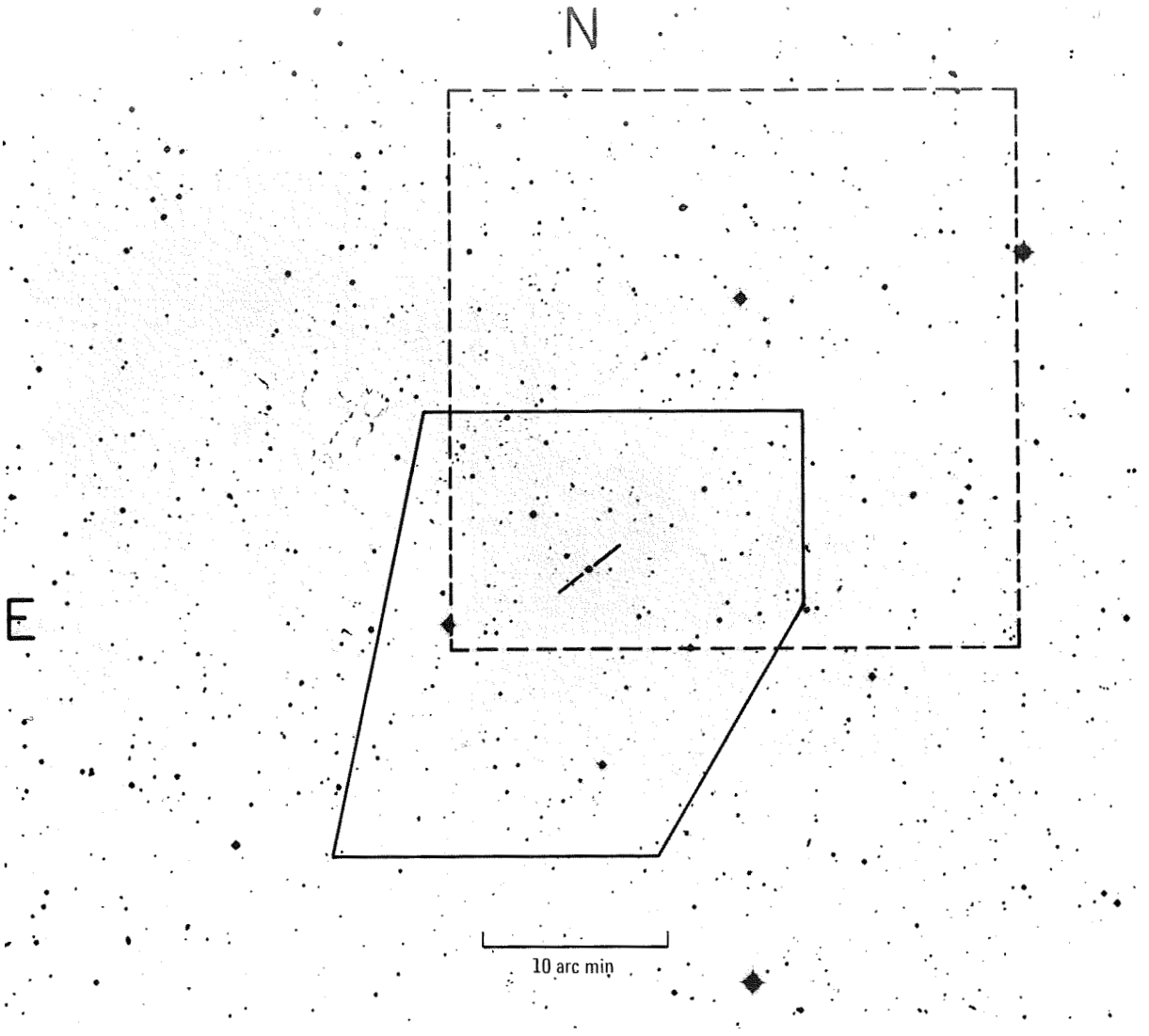

FIGURE 4-5.—Positional error box for the EUV source in Coma Berenices derived from the revolution 109 data (solid line). The broken line is the error box for the soft X-ray source observed from Small Astronomy Satellite-3 (ref. 4-18). The white dwarf HZ 43 is also marked in the center of the photograph. Enlargement is from the blue Sky Survey plate (copyright by the National Geographic Society - Palomar Observatory Sky Survey; reproduced by permission of the Hale Observatories).

blue white dwarf and a faint red comoving companion located 3 arcsecs distant from the white dwarf (see, e.g., ref. 4-20); the two objects are hereafter referred to as HZ 43A, B.

Image tube spectrophotometric measurements at a resolution of approximately 0.8 nm were obtained of HZ 43A, B (composite) and HZ 43A (blue component only), using the Robinson-Wampler image tube scanner (at the Cassegrain focus) of the Lick Observatory 3-m reflector. The resulting spectra of the composite system and HZ 43A are shown in figure 4-7. The difference between these sprectra, also shown in the figure, was used to derive the spectrum of the red star HZ 43B. The HZ 43A spectrum was found to be that of a very hot white dwarf of class DAwk; it lacks the strong spectral lines of singly ionized helium at 541.1 and 468.6 nm evident in the spectrum of

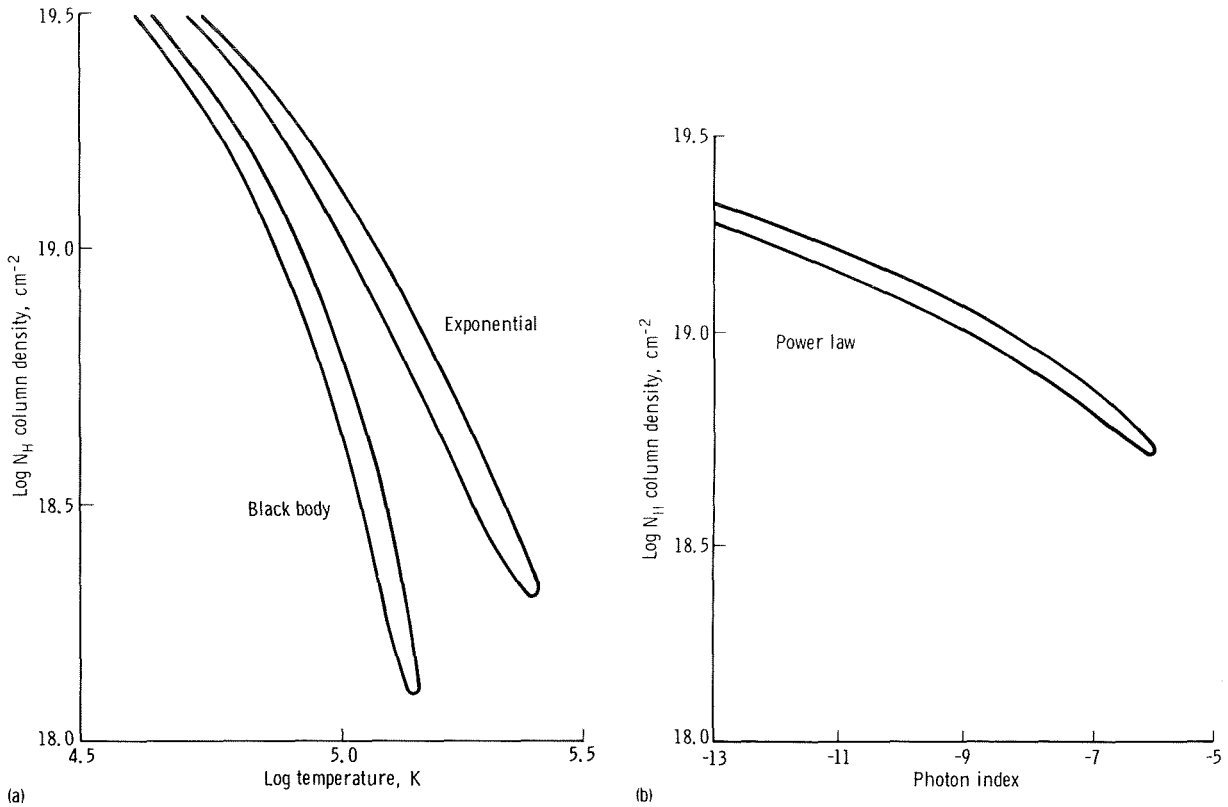

FIGURE 4-6.—Contours of constant χ^2 for the fits of black-body, exponential, and power-law spectra to the HZ 43 EUV data. Each contour has been drawn at the χ^2_{min} + 6.25 level appropriate for 90 percent statistical confidence with three adjustable parameters (ref. 4-19). (a) Black-body and exponential contours. (b) Power-law spectra contour.

DO white dwarfs. No other features other than weak, broad Balmer absorption lines due to neutral hydrogen are evident in the scans of HZ 43A to 680 nm. In particular, none of the spectra show any trace of emission lines, nor has emission ever been reported in the literature for this star, contrary to the assertion of reference 4-18.

The derived HZ 43B spectrum is that of an M-dwarf star with weak Balmer emission lines. The explicit spectral subtype of the star has been estimated in the manner used in reference 4-21, by measuring the strengths of the titanium oxide (TiO) bands and the colors and by visually comparing the overall spectrum with spectroscopic standards. Based on these criteria, HZ 43B is classified as dM3.5. This classification, together with the known absolute brightness of stars of this type and the observed apparent brightness of HZ 43B (fig. 4-7), may be used to derive the distance of the system. The result of this procedure is a distance of 66 (+25, −18) pc.

A new trigonometric parallax has also been derived for HZ 43 using 22 plates obtained at the Allegheny Observatory between 1951 and 1967. The Allegheny material has a poor seasonal distribution, with only five plates obtained at high positive parallax factors; nevertheless, when remeasured and reduced with the latest techniques, the available material is sufficient to yield results of substantially greater accuracy than those in reference 4-22. The new parallax derived is $\pi = 0.015 \pm 0.006$ arcsec. Recently, the U.S. Naval Observatory measured and reduced 21 plates obtained on HZ 43 with their 1.55-m reflector and found a preliminary parallax of $\pi = 0.017 \pm 0.005$ arcsec. The agreement with the

Allegheny value is good, so the results may be combined to derive a weighted mean result of $\pi = 0.016 \pm 0.004$ arcsec, indicating a distance of 62 (+21, −12) pc, which is in excellent agreement with the independently derived distance for HZ 43B previously described.

If the identification of the EUV object with HZ 43A is accepted, the optical and EUV data cited earlier may be combined to derive many interesting parameters of the system (see, e.g., ref. 4-23). A measurement of the monochromatic intensity of a black body at any wavelength yields a locus in a plane (solid angle, effective temperature). In figure 4-8, the EUV and optical data are combined in such a plane. Using the spectrophotometry of HZ 43A shown in figure 4-7, absolute fluxes at the top of the Earth's atmosphere have been derived at five wavelengths in the 400- to 650-nm range. Care was taken to extract each measurement at a wavelength that was free of absorption features and thus truly applicable to the stellar continuum. The loci resulting from these intensity measurements appear in figure 4-8 as the approximately horizontal lines. The ordinate of the graph is the dimensionless ratio, stellar radius to stellar distance; an additional ordinate scale of stellar radius in kilometers is provided, assuming the parallax $\pi = 0.016$ arcsec.

Several interesting features are immediately apparent from the optical data. The loci computed from the different optical wavelengths are not precisely coincident or congruent, undoubtedly reflecting scatter in the observational material. However, they do define a reasonably narrow

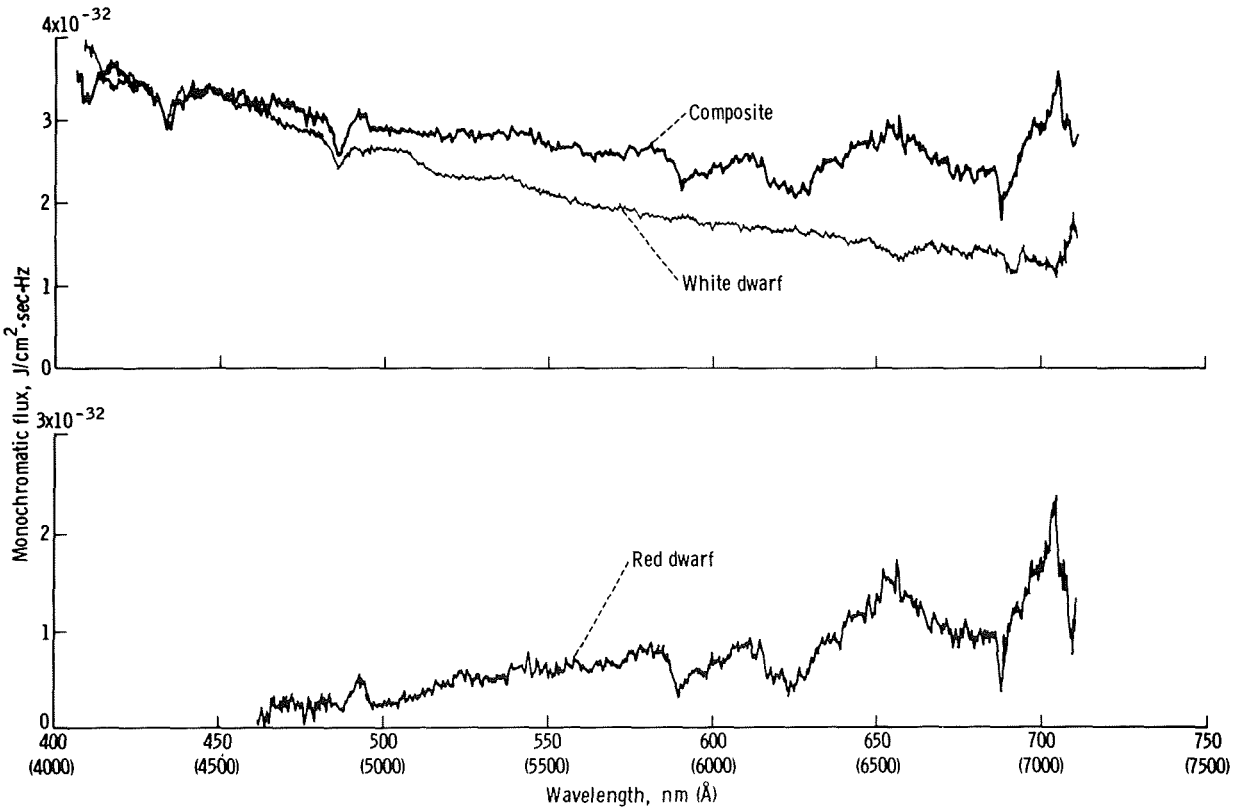

FIGURE 4-7.—Spectrophotometry of HZ 43 obtained with the image tube scanner of the Lick Observatory 3-m telescope, with 0.8-nm resolution. In the upper spectrum, the slit included both red and blue components of the system; the middle spectrum is that of the blue star only. The spectrum of the red component (lower spectrum) was derived by differencing the upper two spectra.

band that is nearly parallel to the temperature axis. This figure thus quantitatively verifies the qualitative knowledge that optical spectrophotometry is very insensitive to the precise temperature of such a hot object. Specifically, the difference in the slopes of black-body spectra at temperatures of 50 000 and 100 000 K is only ≈ 0.1 magnitude across the visible band, which explains the difficulty of determining such a temperature in the optical band.

Ideally, one would want to have monochromatic EUV magnitudes to compare with these optical data. At the moment, however, the only EUV data available are the broadband photometric measurements made during the Apollo-Soyuz mission. Therefore, the data shown in figure 4-6 were used to determine the parameters of five different black-body models that represent the extremes of the allowable values of the adjustable parameters. The resulting intensities were then used to define the EUV locus shown in figure 4-8. The EUV and optical data intersect and provide a common region in the plane (radius, temperature). Further, the EUV data are obviously very sensitive to temperature. The combination of the EUV and optical data accurately defines a small region of allowable effective temperature at 110 000 $\pm$10 000 K and radius of 5000 $\pm$1000 km, under the assumption of this simple black-body emission model. For such an object, the luminosity is 6.8 $L_\odot$, where $L_\odot$ is the solar luminosity, 3.83×10^{26} J/sec. These parameters are in reasonable agreement with white dwarf models; they would give to HZ 43 the highest temperature of any known white dwarf.

Using these stellar parameters, the EUV spectrum may be used to derive the equivalent column density of neutral interstellar hydrogen N_H in the line of sight to HZ 43. This value is $N_H = 4 \times 10^{18}$ atoms/cm^2 or, using the parallax $\pi = 0.016$ arcsec, a volume density of 0.02 atom/cm^3 is derived. This value for the volume density, although lower than many previous suggestions, is consistent with observations of stellar Lyman-alpha 121.6-nm absorption in nearby stars.

A summary spectrum of HZ 43A at all wavelengths thus far measured appears in figure 4-9. The EUV data from the Apollo-Soyuz mission are plotted as the heavy points, and the optical spectrophotometric data shown in figure 4-7 are plotted as the broken line. The radio data from reference 4-24, the UV data from reference 4-25, and the soft X-ray data from reference 4-17 are also included.

It is quite possible that the emergent spectrum of HZ 43A is considerably more complex than the simple black-body spectrum used for these calculations. However, no calculations of high temperature, high surface gravity, and pure hydrogen model atmospheres have been published. Such models are particularly important to assess the effect of wavelength-dependent opacity mechanisms, the Lyman discontinuity, and the presence of trace amounts of atmospheric helium and heavy elements. Preliminary calculations by the authors suggest that these effects may combine to lower the effective temperature from that derived in a black-body approximation.

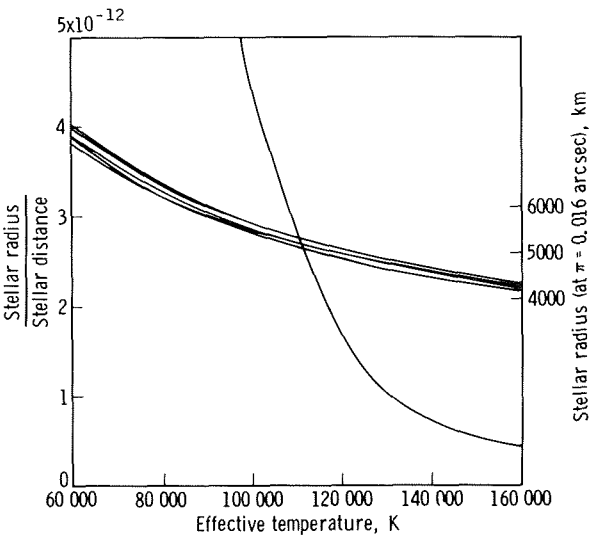

FIGURE 4-8.—Constraints on solid angle as a function of temperature for HZ 43A using the spectra shown in figure 4-7 and the EUV data in figure 4-6, under the assumption of a black-body emission model. The inferred stellar radius at the optimum parallax is also indicated.

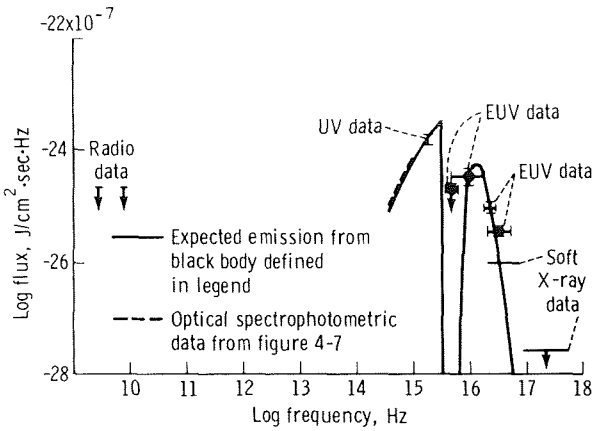

FIGURE 4-9.—The intensity of HZ 43 as observed from Earth. The solid line is the expected emission from a black body of 110 000 K effective temperature attenuated below the Lyman limit by interstellar photoelectric absorption equivalent to $N_H = 4 \times 10^{18}$ atoms/cm^2, using the EUV photoelectric cross sections in reference 4-8.

Feige 24

On revolution 89, a preplanned observation of the hot white dwarf Feige 24 was conducted. Data telemetered during this maneuver are displayed in figure 4-10. The lowest portion of the figure displays the angular offset of the center of the FOV of the EUV telescope from Feige 24 as a function of time. These data are determined by the CMC independently of the EUV experiment. The horizontal broken line denotes the 1.2° radius of the telescope field; thus, all times located between the intersection of this line with the offset graph are times when Feige 24 was within the FOV. This interval is projected onto the time axis of the figure with the vertical broken lines.

Count rate data from the EUV telescope are displayed in the upper portion of figure 4-10. The opaque shutter data show that the detector internal background remained steady at 0.4 count/sec during the entire observation. Data from the 5.5 to 15, 11.4 to 15, and 135 to 154 nm bands have been omitted for clarity; however, they were also constant during the entire maneuver sequence, with mean rates of 3.4, 1.5, and 600 counts/sec, respectively. The strong increases in the 17- to 62- and 50- to 78-nm count rates (cf. fig. 4-10) were due to spatial variations in the geocoronal foreground radiation. This smooth variation as the CSM moves from orbital midnight to sunrise was repeatedly observed on numerous revolutions. (See figure 4-3 for an additional example.)

Figure 4-10 indicates that Feige 24 was within the telescope FOV for 2 minutes commencing at 15:50 UT. Simultaneous with the entrance of the star into the field, a sudden and large increase (200 counts/sec) was observed in the 17- to 62-nm counting rate above the geocoronal background. This new rate persisted for 122 seconds and then fell quickly (within two data samples) to a smooth extrapolation of the geocoronal count rate, exactly simultaneous with the motion of the CSM away from Feige 24. The excess number of counts

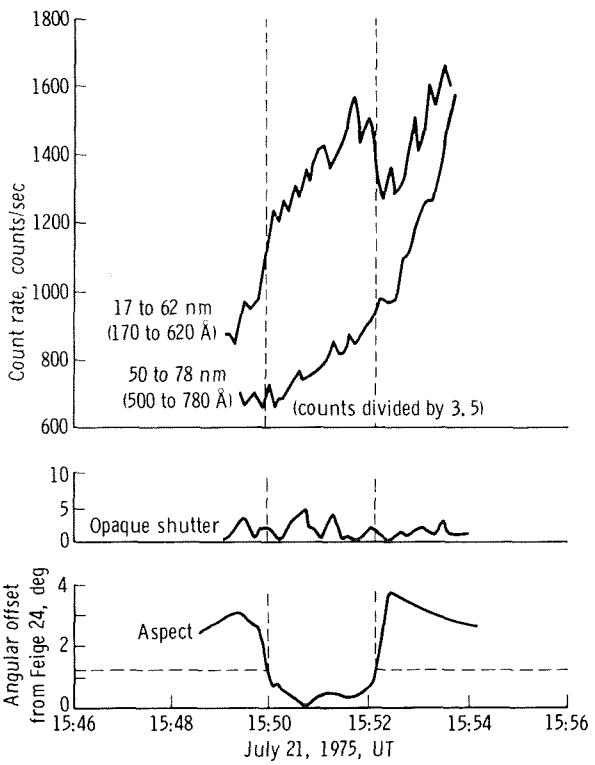

FIGURE 4-10.—Observations of the hot white dwarf Feige 24 made during the Apollo-Soyuz mission. The horizontal broken line indicates the threshold of the telescope 1.2° radius FOV; the projected vertical lines therefore encompass times when Feige 24 was within the FOV.

above the smooth background curve during this 2-minute period was 25 000 ± 550, which is statistically significant at the 45 standard-deviation level. It is concluded with high confidence that an intense celestial source of EUV radiation has been detected at or very near Feige 24. The observed excess flux, when corrected (a 14-percent correction) for residual atmospheric absorption, corresponds to 3 pW/m^2 in the 17- to 62-nm band incident above the Earth's atmosphere. This is comparable to the observed intensity of HZ 43 on revolution 109. There is no evidence for nonstatistical intensity variations during the observation.

In the four other wavelength bands, upper limits to the source intensity may be obtained. In the 5.5- to 15- and 11.4- to 15-nm bands, these limits are 0.10 and 0.17 pW/m^2, respectively, or approximately 10 percent of the observed intensity of HZ 43. It is thus clear that this source has a spectrum substantially steeper than that of HZ 43. The derived upper limit in the 50- to 78-nm band is 0.41 pW/m^2, and the upper limit in the 135- to 154-nm band is 44 pW/m^2, equivalent to the monochromatic magnitude of $m_v > 8.1$ at 137 nm.

The investigators used the detailed laboratory calibration of the FOV dimensions, together with the telemetered count rate and aspect histories and the observation of several known early-type stars in the 135- to 154-nm band, to derive quantitative limits on the position of the EUV source. This position is restricted to a quadrilateral whose corners have epoch 1950 (α, δ): (2^h30^m, 3°15′), (2^h37^m, 5°00′), (2^h42^m, 3°55′), and (2^h35^m, 2°10′). This area (3.8 deg^2) contains Feige 24 at $2^h32.5^m$, 3°31′ and also the hot subdwarf O star Feige 26. The detailed maneuver history of the spacecraft makes Feige 26 an unfavorable candidate, although it cannot be completely excluded on positional grounds alone. However, if the subdwarf classification is correct, Feige 26 is almost certainly too distant to be the source observed, based on interstellar photoelectric opacity; e.g., a distance of 250 pc is suggested in reference 4-3. The observations of BD +28°4211 made during the EUV experiment on revolutions 90 and 105 also suggest that Feige 26 was not the observed source. The star BD +28°4211 is a subdwarf O of a similar optical spectrum but 2 magnitudes brighter than and thus almost certainly closer than Feige 26. The star BD +28°4211 was not detected during the EUV experiment with an upper limit in the 17- to 62-nm band of 0.6 pW/m^2, i.e., 20 percent of the flux from the source discussed here.

Without assuming the optical identification of this source, one may fit simple continuous emission models to the EUV data and constrain parameters of these models to avoid violating the observed fluxes and upper limits. This fitting procedure has been performed in a manner similar to that described earlier for HZ 43. The intensity, temperature or slope, and intervening column density of neutral hydrogen are left as free parameters in the analysis. The results are given in figure 4-11, where contours of constant χ^2 for power-law, exponential, and black-body models are given, analogous to figure 4-6 for HZ 43. This figure provides quantitative confirmation of the qualitative impression yielded by the count-rate ratio of Feige 24 to HZ 43. Feige 24 is a significantly cooler source in thermal models or has a steeper spectrum in power-law models.

The Feige 24 system is known spectroscopically to consist of a very blue DA white dwarf and an unresolved red dwarf M companion. The similarity of this system to HZ 43 immediately suggests that similar mechanisms may produce the observed EUV flux: thermal emission from the degenerate component of the system. Again, the same problem arises as for the analysis of HZ 43 — there are no published relevant model atmospheres for this combination of temperature, gravity, and composition.

In an initial attempt to understand the origin of the EUV emission from Feige 24, spectrophotometric measurements at a resolution of 0.8 nm were obtained of the star using the Cassegrain scanner of the Lick Observatory 3-m reflector. Nine observations were obtained between August 1975 and January 1976. A good signal-to-noise ratio was achieved in all cases, but wavelength coverage was dependent on other observing programs. Blue spectra (380 to 600 nm) data were obtained on August 11 and 12, 1975, and January 8 and 9, 1976. Yellow scans (480 to 720 nm) were acquired on August 11 and 12, 1975, September 2, 1975, and January 7 and 9, 1976. Finally, red and

infrared observations were made on August 12, 1975, and January 7, 1976, to extend wavelength coverage to 820 nm.

The spectrophotometry of Feige 24 is displayed in figure 4-12. Balmer emission lines due to neutral hydrogen appear in most of the scans but are highly variable in strength. When the hydrogen-alpha 685.3-nm line is strongest in emission, the neutral helium lines at 587.6, 447.1, and 667.8 nm also appear in emission. There is no trace of the ionized helium 468.6-nm line reported on one plate of Feige 24 in reference 4-20.

It is obvious from figure 4-12 that Feige 24 has an unusually variable spectrum on the time scale of days. Particularly noteworthy is the apparent anticorrelation of the M-star absorption features with the Balmer emission lines. The spectrum with strongest emission (January 9, 1976) also has the weakest TiO and sodium features, and these latter features are strongest on nights of weakest emission (e.g., August 12, 1975). Whether this activity is due to flare star activity of the dwarf M component or to a heating (possibly periodic) of the M star by the hot white dwarf is as yet uncertain.

In a manner similar to that used in making calculations for HZ 43, the spectrophotometric data of figure 4-12 may be used to classify the M component of the Feige 24 system and to obtain a distance estimate. Based on the equivalent widths of the TiO bands in these data, the red star is of type dM1.5, yielding a distance estimate of 90 (+53, −33) pc. When combined with the EUV data of figure 4-11, this distance implies a volume density of neutral interstellar hydrogen n_H in this direction of $0.01 \lesssim n_H \lesssim 0.1$ atom/cm^3.

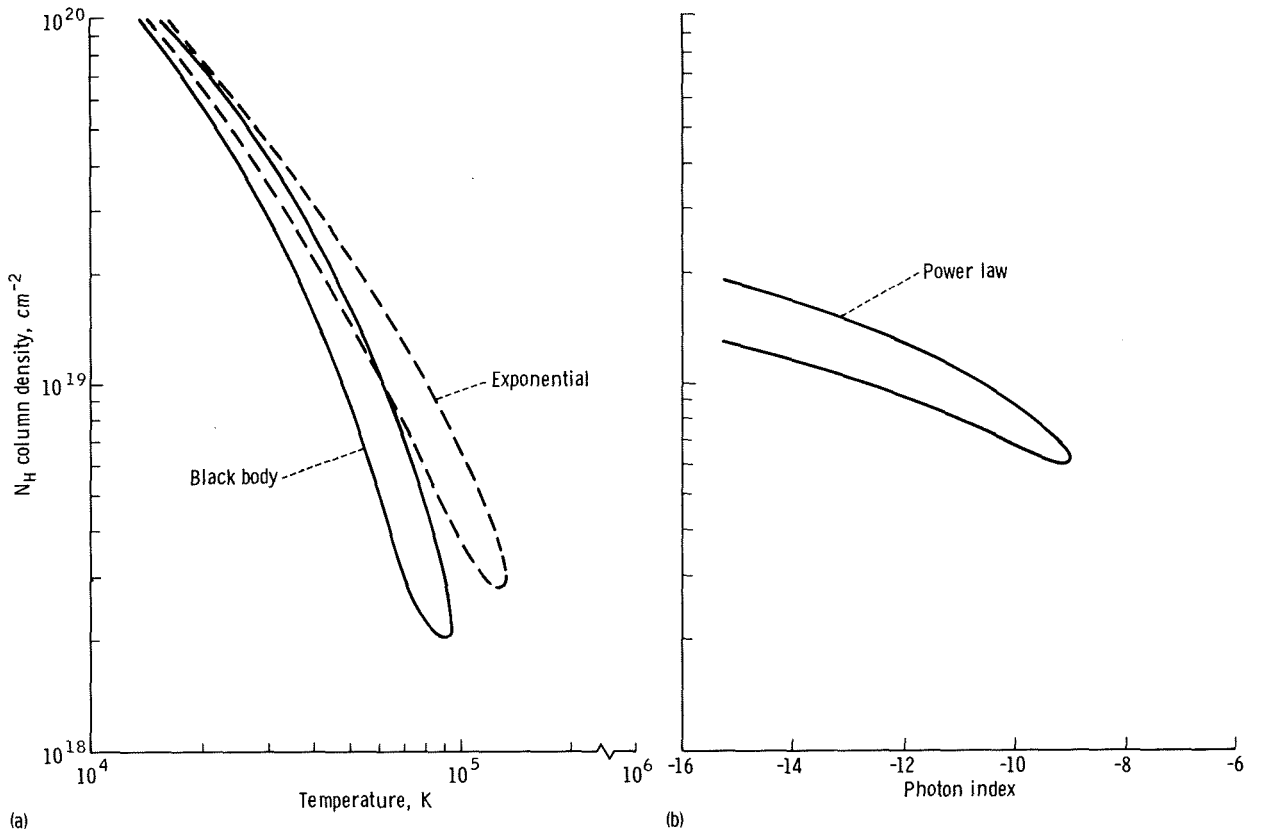

FIGURE 4-11.—Contours of constant χ^2 for fits of black-body, exponential, and power-law spectra to the Feige 24 EUV data. Each contour is drawn at the 90-percent statistical confidence level, analogous to figure 4-6. (a) Black-body and exponential contours. (b) Power-law spectra contour.

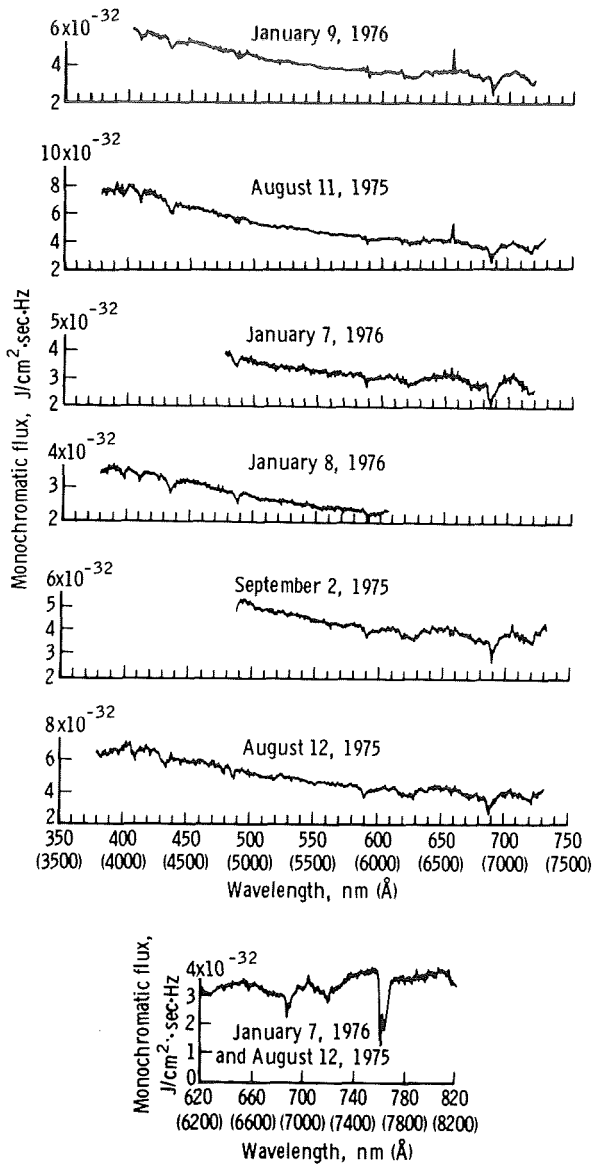

FIGURE 4-12.—Spectrophotometry of Feige 24 obtained with the image tube scanner of the 3-m telescope at the Lick Observatory. Note the prominent and variable emission feature due to neutral hydrogen at 656.3 nm. The deep absorption features at 690 and 760 nm are due to the Earth's atmosphere. (Insert at bottom shows curve of infrared data for two separate nights that have been summed for greater precision.)

Proxima Centauri

On revolutions 94 and 109, the EUV observing program included the target Proxima Centauri, an 11th magnitude M5 dwarf star. At a distance of 1.3 pc, this object has the distinction of being the closest star to Earth other than the Sun. Table 4-III indicates that on revolution 94 there was no positive detection of flux from Proxima Centauri in any of the filters, although sensitivity was somewhat degraded by an intense South Atlantic Anomaly passage on this revolution. However, on revolution 109 there was a very strong positive detection of the target in the 5.5- to 15-nm (Parylene N) band. The data from this observation are given in figure 4-13. The rise and fall of the 5.5- to 15-nm count rates are seen to be precisely coincident with the entrance and exit of Proxima Centauri into and out of the EUV FOV; there can therefore be little doubt of the celestial nature of the detected radiation, or its identification with a source at or very near Proxima Centauri. The nearby companion α Centauri can definitely be eliminated as the identification of the observed source. The spacing between the two stars is 2.2°, and the CSM ephemeris supplied by the NASA Lyndon B. Johnson Space Center indicates that, on this revolution, the EUV experiment received only a 5-second exposure to α Centauri, which occurred just before the observed

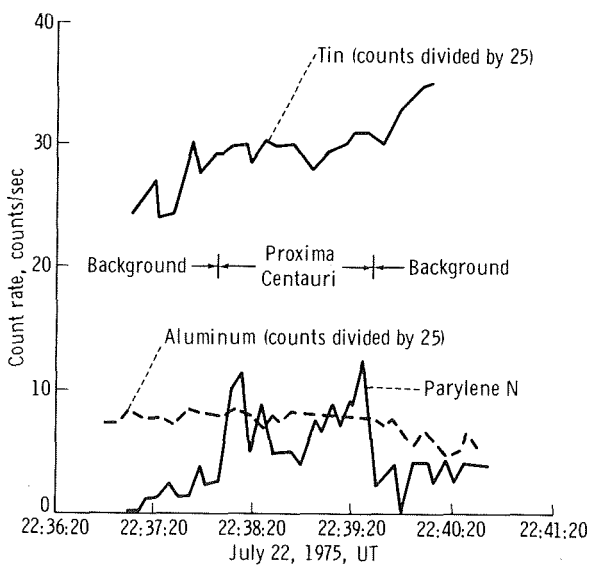

FIGURE 4-13.—Count rates from the EUV telescope during the observation of Proxima Centauri on revolution 109. The times when the star was within the telescope FOV, as computed from the CSM ephemeris, are also indicated.

increase in the 5.5- to 15-nm count rate that persisted for 80 seconds.

Data in figure 4-13 indicate that the source is not detected in the 17- to 62- or 50- to 78-nm bands. The 11.4- to 15-nm data have been omitted for clarity, but they give no statistically significant evidence for a detection. The upper limit in the 11.4- to 15-nm band is consistent with the positive flux detection in the 5.5- to 15-nm region, given the large difference in sensitivity of the parylene filter and the beryllium filter (a factor of 10 assuming a flat incident spectrum).

The revolution 109 data may be used to derive a crude spectrum for the observed source, using the technique previously described for HZ 43 and Feige 24. The results of the spectral fitting procedure are given in figure 4-14. The derivable constraints are all lower limits on the source temperature or spectral hardness, due to the weak nature of the detection. Nevertheless, it is clear from figure 4-14 that this source is quite different from those associated with HZ 43 and Feige 24, in that the spectrum is considerably harder. The flux observed at Earth in the 5.5- to 15-nm band is 0.2 pW/m^2, corresponding to an absolute luminosity of 4.2×10^{21} J/sec or 10^{-5} $L_\odot$ at the 1.3-pc distance of Proxima Centauri.

There is little doubt that a source of this intensity in the 5.5- to 15-nm band would have been detected during the EUV observations on revolution 94. Table 4-III indicates that the upper limit on that occasion was 25 percent of the flux later observed on revolution 109. It is thus concluded with high probability that this source is variable in intensity on at least a time scale of 1 day. This variability and the nature of Proxima Centauri immediately suggest the occurrence of a stellar flare as an explanation for the observed flux. Proxima Centauri is a known optical flare star, and the luminosity of the visible flare events (300 to 700 nm) is similar to the EUV luminosity of the event observed during the Apollo-Soyuz mission.

Conclusive evidence for this hypothesis would, of course, be the simultaneous observation of an optical/EUV flare event. The time of the revolution 109 observation was such that ground-based observations of Proxima Centauri were possible only from the Eastern Hemisphere, south of the Equator. Prior arrangements were in fact made for simultaneous optical photometry to be conducted from the Lake Tekapo, New Zealand, Mount John Observatory of the University of Canterbury; unfortunately, a major snowstorm at this time precluded any observations.

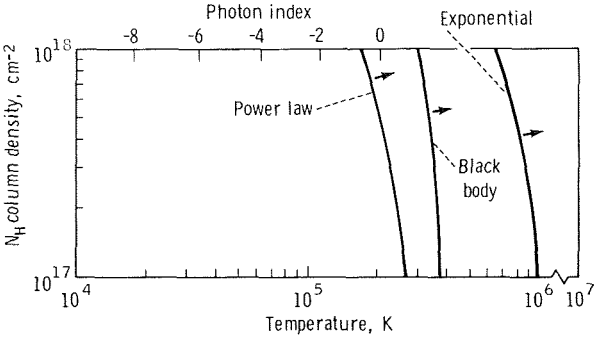

FIGURE 4-14.—Constraints on the EUV spectra of Proxima Centauri derived from the revolution 109 data. The arrows indicate that the spectral parameters must be to the right of the solid lines.

SS Cygni

The bright dwarf nova SS Cygni was observed three times (revolutions 80, 90, and 105) during the mission. Fortunately, the object was undergoing an optical outburst at the time and was therefore 4 magnitudes (a factor of 40) brighter than normal in the visible band. Table 4-III indicates that there is a positive detection of SS Cygni in the 5.5- to 15-nm band on revolution 80, a marginal detection in this band on revolution 90, and no observable flux on revolution 105. There is no evidence for positive fluxes in any of the other band passes on any of the three observations. As is the case with Proxima Centauri, the lack of flux in the 11.5- to 15-nm band is consistent with the detection in the 5.5- to 15-nm channel because of the sensitivity ratios of the two filters.

The revolution 80 data have been used to derive constraints in the incident spectrum, and these results appear in figure 4-15. Note that the spectrum resembles that of Proxima Centauri more than HZ 43 or Feige 24; the source has a flat,

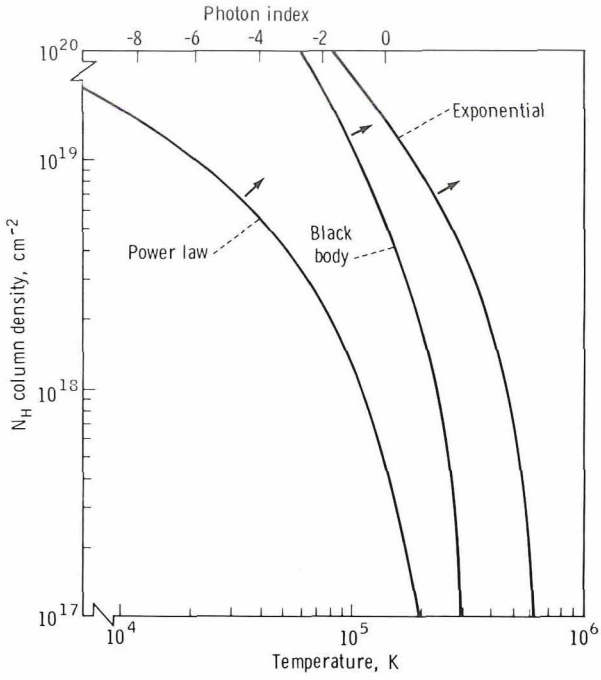

FIGURE 4-15.—Constraints on the EUV spectra of SS Cygni derived from the revolution 80 data. The arrows indicate that the spectral parameters must be to the right of the solid lines.

hard spectrum. The observed flux in the 5.5- to 15-nm range is 0.1 pW/m^2. Because the distance to SS Cygni can only be poorly estimated, it is difficult to accurately compute the interstellar absorption correction and intrinsic luminosity. If the distance to the star is assumed to be 100 pc and the volume density of neutral hydrogen is as low as 0.1 $atom/cm^3$, an absorption correction within the 5.5- to 15-nm range and an intrinsic luminosity of 0.3 $L_\odot$ or 1×10^{25} J/sec can be inferred. This is considerably less than the intensity reported in the 4.4- to 8.3-nm band in reference 4-26 but not incompatible with more recent unpublished observations by the Small Astronomy Satellite-3 and Astronomical Netherlands Satellite (ANS) experiments. It seems likely that there may be a range of possible EUV/soft X-ray luminosities for this system, both in active and quiescent states.

The fact that the Apollo-Soyuz observations spanned almost 2 days presented the opportunity to search for correlations between the EUV and the variable optical intensity. A large volume of optical photometry was successfully acquired for SS Cygni, simultaneous with the Apollo-Soyuz observations. These data include photoelectric photometry with the 0.6-m reflector at the Lick Observatory, photographic photometry with the 0.8-m reflector at the Leuschner Observatory, photoelectric photometry with the 0.8-m reflector at the Manastash Ridge Observatory, and several hundred visual magnitudes supplied by the American Association of Variable Star Observers and numerous independent professional and amateur observers. Interpretation of this large amount of heterogeneous data is not yet complete; however, preliminary results indicate that the optical outburst began on July 17, 1975, and that the system remained at or near maximum light throughout the EUV observations. It is hoped that the joint analysis of the EUV and visible data will ultimately contribute to an understanding of the cause of the outbursts.

Selected Upper Limits

The upper limits on EUV and ultrasoft X-ray emission obtained on many of the sources in table 4-II, which were observed but not detected, provide useful new constraints on models of these objects. Detailed analysis is still underway for most of these objects, but some of the more potentially interesting results will be noted here as examples of the usefulness of the data.

Extreme ultraviolet observations of Sirius B were obtained on revolution 88. This object is important because it is the closest known white dwarf, one of the hottest, and one of only three white dwarfs with dynamically determined masses. This is one of the few objects observed during the Apollo-Soyuz mission that is so close to Earth that interstellar photoelectric opacity is negligible, even at wavelengths as long as the Lyman limit (91.2 nm). The derived upper limit in the 50- to 78-nm band is 1.7 pW/m^2, corresponding to an intrinsic luminosity of 1.4×10^{23} J/sec at a distance of 2.7 pc to Sirius B. This limit is a full factor of 10 more stringent than that derived by the California Institute of Technology investigators in a sounding rocket experiment (ref. 4-27). Preliminary calculations indicate the

Apollo-Soyuz upper limit violates the predicted EUV flux for the currently accepted Sirius B model atmosphere, indicating that these theoretical models may need to be reexamined.

On revolutions 89 and 109, three radio pulsars were observed: PSR 1133+16, 1451−68, and 1929+10. There were no positive detections, with upper limits of approximately 0.2 pW/m^2 obtained in the 5.5- to 15-nm band. These results are interesting because there has never been a detection of thermal radiation from a neutron star. The fact that such objects are not strong thermal X-ray sources in the 0.1- to 1-nm band constrains their surface temperatures to be less than 5×10^6 K (e.g., ref. 4-28); however, until the current experiment, it has been impossible to push this limit to cooler temperatures, and thus more restrictive inferences on the equation of state, because the bulk of thermal radiation for $5 \times 10^4 < T < 5 \times 10^6$ K emerges in the EUV. The Apollo-Soyuz limits may be interpreted to provide these new constraints.

On revolution 104, the binary X-ray pulsar Hercules X-1 was observed in conjunction with a soft X-ray observation. The binary phase of the pulsar during the observation was 0.72, which means that the X-ray source was uneclipsed as viewed from Earth. The source was not detected by either experiment, with the EUV experiment providing an upper limit of 50 fW/m^2 in the 5.5- to 15-nm range. This limit is highly significant because it is substantially less than the positively detected intensity in this band obtained by two sounding rocket experiments (refs. 4-29 and 4-30). As reported in reference 4-29, for example, an intensity of 2 pW/m^2 was observed in the 4.4- to 6.9-nm band, or a factor of 40 above the upper limit. This proves that the ultrasoft X-ray component of Hercules X-1 is time variable, perhaps as a function of the 35-day period of the system.

Observations of the Diffuse Background Radiation

Although the 4.4- to 6-nm component of the cosmic diffuse background radiation was discovered almost a decade ago (ref. 4-31), its origin is still not understood. This radiation is spatially anisotropic, in contrast to the diffuse X-ray background at shorter wavelengths. Also, the flux is detected in directions where the mean free path due to interstellar photoelectric opacity is known to be small. These facts indicate that this radiation is distinct from the hard X-ray background and has a relatively local galactic origin. Various investigators have searched for correlations of the intensity of this radiation with numerous other phenomena (e.g., neutral interstellar hydrogen column density, far-UV absorption lines of hot interstellar gas, low-frequency radio features, etc.) with ambiguous results. Part of the difficulty is the lack of a high-resolution all-sky survey at those wavelengths made with one instrument over a relatively short period of time.

The Apollo-Soyuz EUV observations in the 5.5- to 15-nm band represent a tremendous increase in the data available to examine this problem. A combination of data acquired during operations at or near the preselected EUV targets, during the Helium Glow Experiment great circle scans, and during the soft X-ray maneuvers encompasses a remarkably representative sample of all galactic longitudes and latitudes. The observations were made primarily with the 2.4°-diameter FOV, which was the best spatial resolution ever used for such a survey, and were all acquired by the same instrument over a period of time that was short compared to many solar and terrestrial phenomena. The data also extend to longer wavelengths than previously used for this work to take advantage of the sharply increasing fluxes due to the steep spectrum. Finally, data were acquired at a wide variety of different geocentric, geomagnetic, and solar coordinates, enabling a careful search to be made for noncelestial flux contributions that have been a problem in many previous brief experiments.

The reduction of this large amount of data is still underway; however, preliminary results appear in figure 4-16, where the 5.5- to 15-nm count rate (with opaque shutter background subtracted) is plotted as a function of galactic latitude for a variety of longitudes. Several interesting features are apparent in figure 4-16. Even using data strictly from EUV targeted observations, a remarkably wide spatial coverage was achieved in

galactic coordinates. To within the counting statistics of the observations, the intensity seems reasonably uniform as a function of longitude and latitude. This is in sharp contrast to 4.4- to 6-nm surveys (e.g., ref. 4-32) in which high-to-low latitude intensity contrasts of a factor of 5 are not uncommon. Thus, these data are interpreted as evidence that spatial isotropy may be gradually restored as observations are shifted to longer and longer wavelengths.

A natural (although tentative) interpretation of this phenomenon is as follows. As the wavelength of observation increases, the mean free path due to interstellar photoelectric absorption decreases. If the radiation is in fact due to large-scale galactic features such as thermal emission from hot gas clouds or radio loops, the line of sight at these longer wavelengths will reach only the very nearest such features, which will in turn have the largest solid angles as viewed from Earth. As fewer emitting features are superposed, a large-scale intensity isotropy would be expected to emerge. Further analysis of the EUV background observations will be needed to verify the plausibility of this concept.

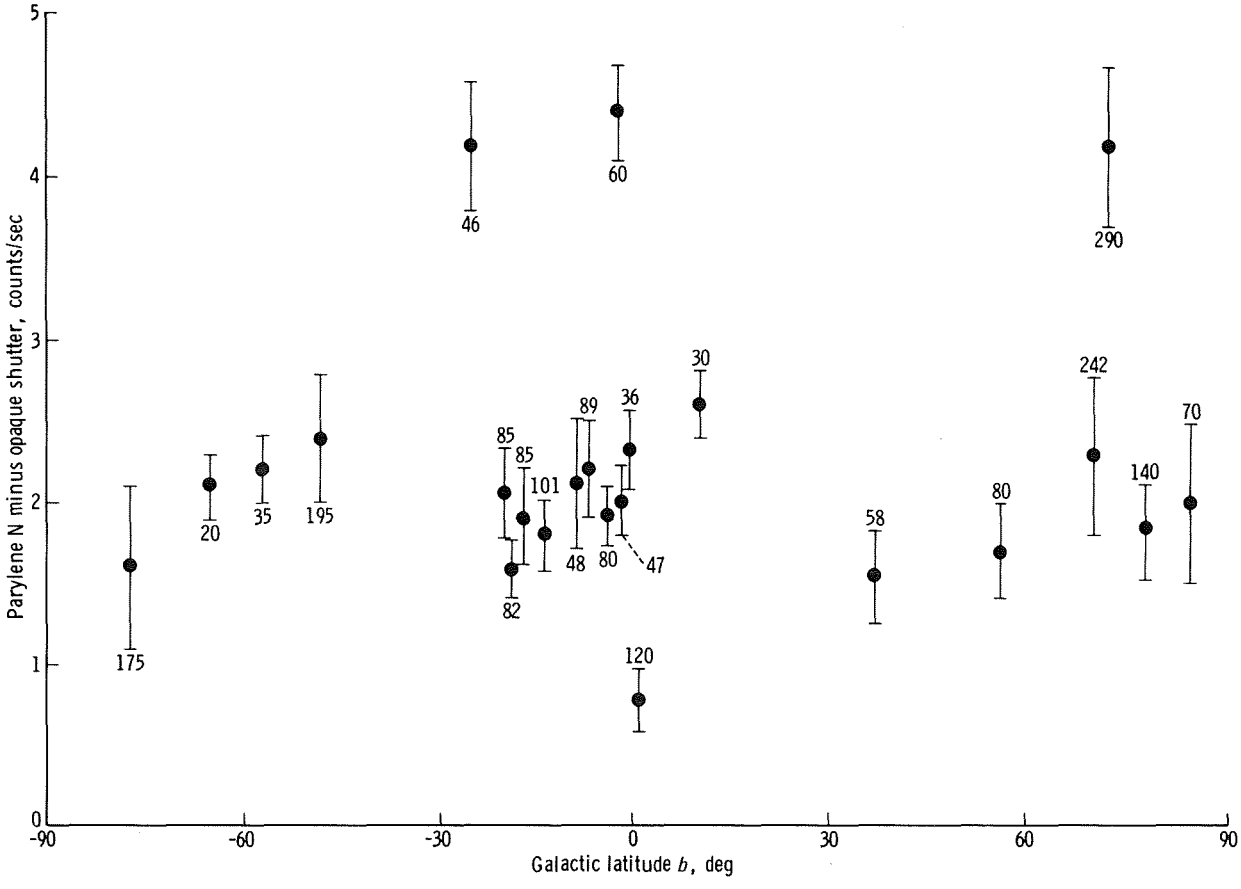

FIGURE 4-16.—The intensity of the diffuse cosmic background radiation in the 5.5- to 15-nm band as a function of galactic latitude, as observed by the EUV telescope. The galactic longitude where each data point was acquired is also indicated.

SUMMARY

All the primary goals of the EUV Survey Experiment were achieved. Data were acquired on 30 different targets belonging to a variety of different classes of stars. Extensive and sensitive data on the EUV background radiation were also obtained. The targeted observations have resulted in the detection of at least four celestial sources of EUV radiation, the first such objects ever to be detected. The observed objects belong to three different classes of stars — hot white dwarfs, flare stars, and dwarf novae — and have different spectra and intrinsic luminosities. The investigators conclude that extrasolar EUV astronomy is not only feasible but that the varied nature of the detectable sources indicates that this field will have an impact on astronomy as a whole comparable to that obtained when previously unexplored windows in the electromagnetic spectrum have been opened.

ACKNOWLEDGMENTS

The Lick Observatory 3-m spectrophotometry discussed here was obtained in collaboration with Dr. J. Liebert (Steward Observatory, University of Arizona) and Dr. H. Spinrad (Astronomy Department, University of California at Berkeley). The parallax for HZ 43 was obtained in collaboration with Dr. G. Gatewood (Allegheny Observatory, University of Pittsburgh).

REFERENCES

4-1. Hills, J. G.: An Explanation of the Cloudy Structure of the Interstellar Medium. Astron. & Astrophys., vol. 17, 1972, pp. 155-160.

4-2. Rose, W. K.; and Wentzel, D. G.: Ultraviolet Stars and the Interstellar Gas. Astrophys. J., vol. 181, 1973, pp. 115-123.

4-3. Greenstein, J. L.; and Sargent, A. I.: The Nature of Faint Blue Stars in the Halo. II. Astrophys. J. Supp. Series, vol. 28, no. 259, 1974, pp. 157-210.

4-4. Carnochan, D. J.; Dworetsky, M. M.; et al.: A Search for Ultraviolet Objects. Phil. Trans. Roy. Soc. London, A, vol. 279, 1975, pp. 479-485.

4-5. Rogerson, J. B.; York, D. G.; et al.: Spectrophotometric Results From the *Copernicus* Satellite. III. Ionization and Composition of the Intercloud Medium. Astrophys. J. (Letters), vol. 181, 1973, pp. L110-L115.

4-6. Bohlin, R. C.: *Copernicus* Observations of Interstellar Absorption at Lyman Alpha. Astrophys. J., vol. 200, 1975, pp. 402-414.

4-7. Dupree, A. K.: Ultraviolet Observations of Alpha Aurigae From *Copernicus*. Astrophys. J. (Letters), vol. 200, 1975, pp. L27-L31.

4-8. Cruddace, R.: Paresce, F.; Bowyer, S.; and Lampton, M.: On the Opacity of the Interstellar Medium to Ultrasoft X-rays and Extreme Ultraviolet Radiation. Astrophys. J., vol. 187, 1974, pp. 497-504.

4-9. Riegler, G. R.; and Garmire, G. P.: Observations of the Extreme Ultraviolet Nightglow. J. Geophys. Res., vol. 79, 1974, pp. 226-232.

4-10. Henry, P.; Bowyer, S.; et al.: An Extreme Ultraviolet Search of the Galactic Anticenter Region. Bull. American Astron. Soc., vol. 6, no. 4, part I, 1974, p. 446.

4-11. Henry, Patrick; Bowyer, Stuart; et al.: Limits on the Space Density of 0 Subdwarfs and Hot White Dwarfs From a Search for Extreme Ultraviolet Sources. Astrophys. J., vol. 205, 1976, pp. 426-429.

4-12. Henry, Patrick; Cruddace, Raymond; et al.: Limits on the Soft X-ray and Extreme Ultraviolet Flux From RX Andromedae and U Geminorum. Astrophys. J. (Letters), vol. 197, 1975, pp. L117-L121.

4-13. Henry, P.; Cruddace, R.; et al.: An Extreme Ultraviolet Search of the North Galactic Polar Region. Astrophys. J., vol. 195, 1975, pp. 107-110.

4-14. Margon, B.; and Bowyer, S.: Extreme Ultraviolet Astronomy From Apollo-Soyuz. Sky and Telescope, vol. 50, no. 1, 1975, pp. 4-9.

4-15. Hoshiko, H. H.: Helical Channel Multiplier Package Design for Space Instrumentation. Rev. Sci. Instr., vol. 46, no. 3, 1975, pp. 331-332.

4-16. Hayakawa, Satio; Tanaka, Yasuo; et al.: Soft X-ray Emission From the Direction of the Coma Cluster. Publ. Astron. Soc. Japan, vol. 27, 1975, pp. 615-617.

4-17. Margon, B.; Malina, R.; et al.: An Ultrasoft X-ray Source in Coma Berenices. Astrophys. J. (Letters), vol. 203, 1976, pp. L25-L28.

4-18. Hearn, D. R.; Richardson, J. A.; et al.: MX 1313+29: A Compact Source of Very Low Energy X-rays in Coma Berenices. Astrophys. J. (Letters), vol. 203, 1976, pp. L21-L24.

4-19. Margon, B.; Lampton, M.; Bowyer, S.; and Cruddace, R.: Soft X-ray Spectroscopy of Three Extragalactic Sources. Astrophys. J., vol. 197, 1975, pp. 25-29.

4-20. Eggen, O. J.; and Greenstein, J. L.: Spectra, Colors, Luminosities, and Motions of the White Dwarfs. Astrophys. J., vol. 141, 1965, pp. 83-108.

4-21. Liebert, James: The Demise of the Degenerate M Stars. Astrophys. J. (Letters), vol. 200, 1975, pp. L95-L98.

4-22. Wagman, N. E.: Photographic Determinations of the Parallaxes of 67 Stars With the Thaw Refractor, Astronom. J., vol. 72, 1967, pp. 957-958.

4-23. Lampton, M.; Margon, B.; et al.: Discovery of a Non-solar Extreme Ultraviolet Source. Astrophys. J. (Letters), vol. 203, 1976, pp. L71-L74.

4-24. Condon, J.: New Soft X-ray Source. International Astronomical Union Circular No. 2790, June 17, 1975.

4-25. Wu, C. C.; Wesselius, P. R.; et al.: HZ 43. International Astronomical Union Circular No. 2805, July 22, 1975.

4-26. Rappaport, S.; Cash, W.; et al.: Possible Detection of Very Soft X-rays from SS Cygni. Astrophys. J. (Letters), vol. 187, 1974, pp. L5-L7.

4-27. Riegler, G. R.; and Garmire, G. P.: Search for Extreme Ultraviolet Radiation From Selected Stars. Astron. & Astrophys., vol. 45, no. 1, 1975, pp. 213-216.

4-28. Greenstein, George; and McClintock, Jeffrey E.: Prospects for Detecting Blackbody X-rays From Neutron Stars. Science, vol. 185, Aug. 9, 1974, pp. 487-490.

4-29. Shulman, S.; Friedman, H.; et al.: Soft X-ray Emission From Hercules X-1. Astrophys. J. (Letters), vol. 199, 1975, pp. L101-L104.

4-30. Catura, R. C.; and Acton, L. W.: Intense Soft X-ray Flux From Hercules X-1. Astrophys. J. (Letters), vol. 202, 1975, pp. L5-L7.

4-31. Bowyer, C. S.; Field, G. B.; and Mack, J. E.: Detection of an Anisotropic Soft X-ray Background Flux. Nature, vol. 217, 1968, pp. 32-34.

4-32. Davidsen, A.; Shulman, S.; et al.: Observations of the Soft X-ray Background. Astrophys. J., vol. 177, 1972, pp. 629-642.